

Article

# Instability Risk Assessment for Deep Excavation of Soil–Rock Combinations Containing Groundwater

Liwei Zhang, Weiguo Zhang, Zaiquan Wang, Sijia Liu \* and Kai Liu

School of Civil Engineering, Qingdao University of Technology, Qingdao 266520, China; zhangliwei@qut.edu.cn (L.Z.); zwgqut@163.com (W.Z.); zqwang4521@163.com (Z.W.); liukai20000101@126.com (K.L.)

\* Correspondence: liusijialyg@126.com

**Abstract:** Dynamic risk assessment is a pivotal tool for enhancing construction safety and minimizing the potential for partial failure during deep and extensive excavation projects. To enhance the efficacy of dynamic risk assessment in deep excavation, this study introduces a novel risk assessment model designed to evaluate instability risk in extensive excavations. It comprises a risk factor selection model for identifying the most pertinent factors and an instability risk assessment model for gauging the extent of instability risk throughout the construction process. Then, the model was deployed in the construction of Anshan Road Station of the Qingdao Metro. To pinpoint the factors with the most pronounced impact on excavation instability, a risk factor selection model was employed, yielding a comprehensive risk evaluation index system. For real-time assessment of risk, the monitoring data were used as the primary source of evidence. A comprehensive comparative analysis involving actual data and predictions from conventional RBF and back propagation neural networks was performed. The outcome of this analysis underscored the superior accuracy and predictive capabilities of the assessment model. The instability risk assessment model offers the ability to dynamically evaluate the instability risk associated with extensive excavations featuring a combination of soil and rock. It can serve as a valuable methodological tool, furnishing essential support for the systematic prevention and mitigation of excavation instability disasters.

**Keywords:** deep excavation; soil–rock combination; theory fusion; dynamic assessment; field monitoring



**Citation:** Zhang, L.; Zhang, W.; Wang, Z.; Liu, S.; Liu, K. Instability Risk Assessment for Deep Excavation of Soil–Rock Combinations Containing Groundwater. *Appl. Sci.* **2023**, *13*, 12887. <https://doi.org/10.3390/app132312887>

Academic Editor: Tiago Miranda

Received: 7 November 2023

Revised: 26 November 2023

Accepted: 28 November 2023

Published: 30 November 2023



**Copyright:** © 2023 by the authors. Licensee MDPI, Basel, Switzerland. This article is an open access article distributed under the terms and conditions of the Creative Commons Attribution (CC BY) license (<https://creativecommons.org/licenses/by/4.0/>).

## 1. Introduction

In recent years, to meet the demands of urban expansion, there has been a notable surge in the construction of deep and extensive excavation projects within densely developed areas. Nevertheless, the excavation process is fraught with the potential for substantial deformations, partial failures, and structural support breakdowns. These issues can be attributed to a range of factors, such as geological conditions, the stability of the support system, and the surrounding environment. Consequently, these challenges not only pose a significant risk to safety, leading to potential casualties, but also contribute to significant delays in the overall construction timeline [1–4]. For example, on 15 November 2008, an excavation collapse occurred in the North 2 excavation of Xianghu Station of Hangzhou Metro Line 1, which caused 21 deaths and a direct economic loss of 49.61 million yuan. Another example, on 15 June 2021, a part of the north side of the excavation of the Bank of Nanjing Science and Education Innovation Park Phase II project in the Nanjing High-Tech Zone experienced a partial collapse accident, which involved casualties and 9.8973 million yuan in direct economic losses. On the other hand, excavation exerts an impact on the surrounding environment that cannot be ignored, especially in urban densely built-up areas, and is prone to triggering problems such as cracking of the surrounding buildings and deformation of road surfaces [5–8]. In addition, on 21 March 2021, the interior of a building excavation in Hangzhou produced an inclined collapse, which caused the destruction of the supporting structure and, meanwhile, contributed to the collapse and displacement

of the adjacent road, where the ground cracks were more than 30 m in length. Although monitoring is commonly employed in engineering to ensure excavation safety, it sometimes lags in its reflection of the safety status. As a result, this has received extensive attention and discussion among researchers, to make a correct assessment of the stability of an excavation during the construction process and to judge the safety status [9–12].

Research about the risk analysis of excavations began in the 1960s, initially focusing on exploring theories, while analyzing the field data of actual projects in certain areas. Finno et al. [13] presented a method of predicting the degree of risk based on the cracks of surrounding buildings to analyze the impact of excavation on the surrounding buildings and used this method to predict the potential risk. Son and Cording [14] classified influencing factors by combining the results of physical modeling and numerical simulation with deformation monitoring data during the actual excavation process, so as to predict the safety of the excavation and the damage to the surrounding buildings. These analyses provide the basis for subsequent risk assessment studies. Additionally, numerous researchers have introduced mathematical models for the analysis of excavation risk and obtained more accurate results [15–17]. Choi et al. [18] presented an underground engineering risk analysis method based on an uncertainty model with fuzzy concepts for analyzing the reliability of excavation projects, which was successfully applied in a Korean subway project. Zhou and Zhang [19] established a fuzzy comprehensive evaluation model using a Bayesian network that could qualitatively judge the safety status of excavations according to the characteristics of uncertainty and fuzziness. Meanwhile, they established a hybrid framework combining the ratio analysis method of stepwise weight assessment and the theory of complex proportion assessment. Zhou et al. [20] substituted different monitoring data and risk level monitoring during construction in a random forest model, on the basis of which an intelligent risk prediction model for subway deep excavation was established and successfully applied. In addition, the failure mechanics of surrounding rocks affected by influencing factors such as anisotropy and heterogeneity have been investigated by researchers [21–24].

With the emergence of artificial intelligence, artificial intelligence learning algorithms based on neural networks have gradually become one of the key methods for geotechnical engineering risk prediction and early warning [25–28]. Zhang et al. [29] proposed a combined prediction model based on an optimized gray discrete Verhulst model and BP neural network and proved its high prediction accuracy and stability by applying the model to predict the settlement of actual building pits. Shen et al. [30] established a comprehensive evaluation index system for the risk of a subway station by analyzing the influencing factors on excavation construction, on the basis of which a three-stage fuzzy comprehensive evaluation model was proposed and the risk level was ranked. Lin et al. [31] proposed a risk assessment model for excavation engineering based on mixed fuzzy set theory, which was successfully applied in actual projects. Sou-Sen and Hsien-Chuang [32] proposed a method based on an artificial neural network for predicting the surface settlement of deep excavation, which was used to evaluate the risk of construction in combination with monitoring data. Li et al. [33] proposed a deep learning model based on a bidirectional long short-term memory neural network combined with self-attention mechanism for predicting the vertical displacement of buildings adjacent to excavation, which was validated using an actual subway project. Lü et al. [34] proposed an analytical method based on artificial neural networks and a uniform design for predicting the probability of damage in deep rock excavations and verified its validity by comparing the results with those of Monte Carlo simulation and a polynomial response surface methodology. Kounlavong et al. [35] analyzed the relationship between different factor variables and the degree of excavation safety with a sensitivity analysis using artificial neural networks. Ning et al. [36] established a real-time online prediction model for surface settlement during foundation excavation based on a long short-term memory neural network with improved quality of input data using grey relational analysis and demonstrated its advantages by applying it to a specific project. Tang et al. [37] proposed a ground settlement prediction model for

predicting the potential risk to the surrounding buildings caused by excavation, which used a BP neural network to predict the settlement, while the validity of the model was verified by comparing the prediction results with the actual data. Tao et al. [38], in order to improve the accuracy of excavation engineering prediction, considering the uncertainty in the nature of geotechnical material, proposed an excavation response model, which learns the relationship between geotechnical material parameters and excavation response through a bidirectional long short-term memory neural network and can realize the rapid prediction of excavation response. Currently, neural network-based prediction models have been widely used in excavation projects, with excellent results [39–42]. Overall, the development and application of risk assessment has helped to reduce the number of engineering accidents.

In the abovementioned research, more attention was paid to a certain project or a certain geological condition with respect to the selection of risk evaluation indexes. Prediction using the existing assessment models is not satisfactory in the Qingdao area due to its unique geological characteristics: a typical upper-soft and lower-hard composite stratum. On the other hand, the choice of risk indexes focuses more on explicit factors such as geological conditions and construction design, making it difficult to dynamically assess the risk of excavation based on these models. To try to resolve this problem, this paper considers monitoring indexes as excavation risk indexes while considering the geological characteristics of Qingdao area, jointly establishing an excavation risk assessment index system. Potential risk factors were identified and filtered based on a useful factor ratio (UR) analysis and combined weights ranking. After the establishment of the risk index system, an improved RBF network with an LLE algorithm was used to predict and evaluate the excavation risk. The validity of the proposed method was verified by conducting a risk assessment of the Anshan Road station pit. This provided an effective dynamic prediction of the excavation risk. The risk assessment model established in this paper evaluates the risk of excavation more accurately and scientifically, which can provide better support for the safe construction of the Qingdao subway.

## 2. Models and Methods

In this paper, a variety of theories, including the analytic hierarchy process, entropy method, grey relational analysis, locally linear embedding, and radial basis function network, are applied to develop the risk assessment model. A brief review of the model and theories is presented below.

### 2.1. Overview of the Assessment Model

The risk assessment model proposed in this paper comprises a risk factor selection model for identifying the most pertinent factors and an instability risk assessment model for gauging the extent of instability risk throughout a construction process. This is roughly divided into three stages when applied, namely stage 1 (factor selection), stage 2 (data handling), and stage 3 (risk assessment), and the detailed assessment process is shown in Figure 1.

As shown in Figure 1, the potential factors affecting the stability of an excavation are first selected, based on analyzing the characteristics of a deep and large excavation with soil–rock combinations, and by combining the relevant specifications, literature research results, and the study of the risk mechanism. Then, the potential factors are screened, in order to construct an instability risk evaluate index system for deep and large excavation with soil–rock combinations, consisting of factors having a greater influence on the stability of the excavation, using a risk factor selection model. After that, we proceed to Stage 2, where the results of the data selection are verified for correctness. Data are not processed by LLE for dimensionality reduction unless the filtering is correct. Finally, in stage 3, the dimensionally reduced processed data are used as input data to the RBF neural network and are calculated to obtain the prediction results.

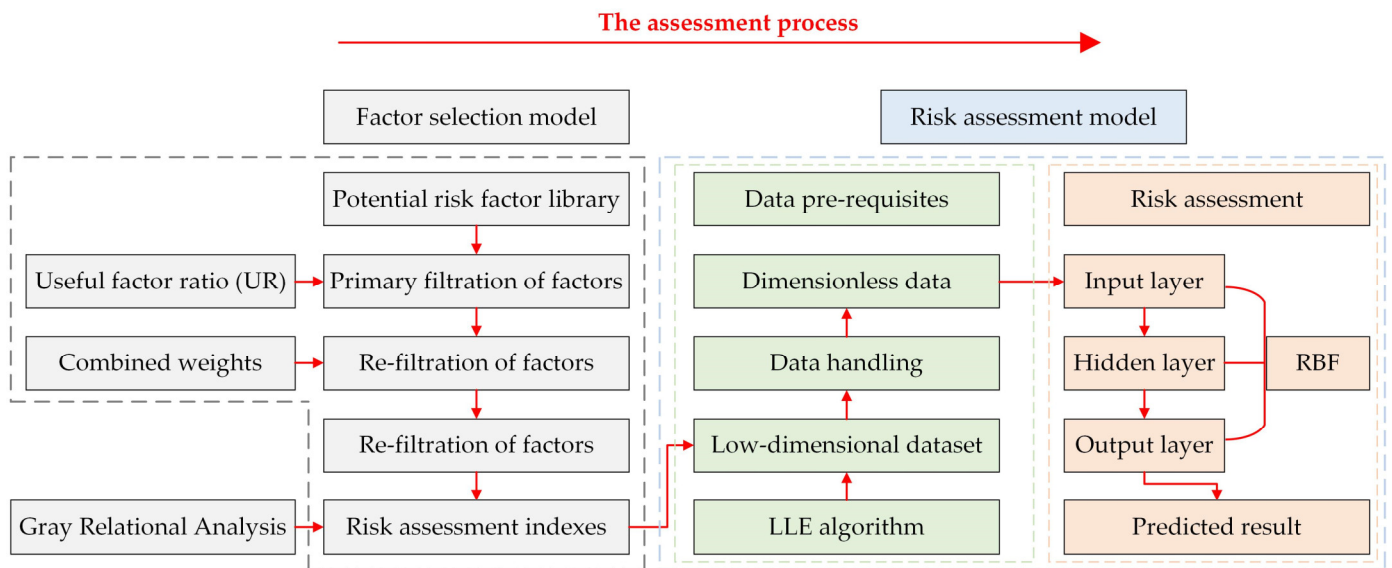


Figure 1. Evaluation process.

In Stage 1, a factor selection model is used to filter potential risk factors. This is composed of a combination of AHP and entropy methods. The selection of factors is based on their combined weights. This combined weighting method can ameliorate the problems of missing factor selection and high subjectivity of weights [43], which was the reason for its selection. In this model, AHP is first used for initial screening of risk factors, followed by the calculation of subjective weights. Meanwhile, the objective weights of factors are obtained by combining the entropy method, in order to calculate their combined weights based on a comprehensive weighting method. The formula for calculating the combined weights is

$$z_i = \alpha w_i + \gamma \beta_i (i = 1, 2, \dots, n) \tag{1}$$

$$\begin{cases} \alpha w_i w_i^T + \gamma w_i \beta_i^T = w_i w_i^T \\ \alpha \beta_i w_i^T + \gamma \beta_i \beta_i^T = \beta_i \beta_i^T \end{cases} \tag{2}$$

where  $z_i$  is the combined weight,  $w_i$  and  $\beta_i$  are the subjective weight and objective weight, and  $\alpha$  and  $\gamma$  are the weighting coefficients. Indeed, calculating the combined weights is difficult when the number of risk factors is excessive. For this reason, prior to factor selection, this paper proposes pre-filtering the factors with the useful factor ratio (UR) to improve the efficiency of stage 1. The UR reflects the degree of importance of the different factors. It is introduced to quantify the survey results based on the judgment of industry experts on the reasonableness of the factor selection and to provide preliminary screening of possible factors influencing the risk. The formula for calculating UR is as follows:

$$UR = \frac{n}{N} \cdot \lambda, \tag{3}$$

where  $n$  is the number of group members who consider the factor essential,  $N$  is the total number of group members, and  $\lambda$  is the coefficient of variation, which takes the value of 0.9. UR values less than 0.4 indicate that the factor is unimportant and will not be involved in further calculations.

In Stage 2 and 3, the risk assessment model is applied. It is composed of a radial basis function (RBF) network and local linear embedding (LLE) algorithm. In particular, these filtered factors are not counted unless they are confirmed as correctly selected through grey relational analysis (GRA).

2.2. Rationale

2.2.1. Analytic Hierarchy Process

AHP is a method of decomposing a complex problem into an ordered recursive hierarchy, on which a mathematical method is used to make decisions. It can contribute to simple decision-making methods for complex decision-making problems with less quantitative information.

The steps for calculating subjective weights using AHP are as follows:

Several experts in the relevant fields were invited to compare a number of risk factors two-by-two and to score them, using the 1–9 scale method with criteria as shown in Table 1.

Table 1. Scoring criteria.

$C_{ij}$	Definition	$C_{ij}$	Definition
1	Equal importance	2	Between weak and equal importance
3	Weak importance	4	Between essential or strong and weak importance
5	Essential or strong importance	6	Between demonstrated and essential or strong
7	Demonstrated importance	8	
9	Absolute importance		

and to construct an indirect judgment matrix,

$$C = (c_{ij})_{n \times n'} \tag{4}$$

to calculate the importance ranking index of each evaluation factor using Equation (3),

$$r_i = \sum_{j=1}^n c_{ij} (i = 1, 2, \dots, n), \tag{5}$$

where  $r_i$  is the importance ranking index of each evaluation factor, and  $c_{ij}$  is the degree of relative importance of the factor  $i$  to the factor  $j$ .  $A_{max}$  denotes the element corresponding to the maximum ranking index,  $A_{min}$  indicates the element corresponding to the minimum ranking index, and the elements of the judgment matrix are

$$b_m = A_{max} / A_{min}. \tag{6}$$

Converting the indirect judgment matrix into a judgment matrix,

$$B = (b_{ij})_{n \times n'} \tag{7}$$

and the formula is

$$b_{ij} = \begin{cases} \frac{r_i - r_j}{r_{max} - r_{min}} (b_m - 1)^2 & r_i > r_j \\ 1 & r_i = r_j \\ \frac{r_i - r_j}{r_{max} - r_{min}} (b_m - 1)^2 + 1 & r_i < r_j \end{cases} \tag{8}$$

where  $b_{ij}$  is the degree of importance of  $i$  evaluation factor to  $j$  evaluation factor, and  $b_m$  is the ratio of  $A_{max}$  to  $A_{min}$ , where  $(b_m - 1)^2$  serves as a squared term to describe the magnitude of the span of the ranking index  $A$  and ensures that the maximal ranking index approaches the minimal ranking index converging to 1.

According to matrix theory, the weight value of each index is the judgment matrix eigenvector. Calculated by normalizing the elements in  $B$  by columns, the formula obtained is

$$w_i = \frac{\bar{w}_i \varphi_i}{\sum_{i=1}^n \bar{w}_i \varphi_i} (i = 1, 2, \dots, n), \tag{9}$$

where  $w_i$  is the subjective weight of each layer of risk factors, and  $\varphi_i$  is the modified coefficient, whose value is selected depending on the difference between the maximum

value and the minimum value in each column (row). When the difference is greater than 0 and less than 1, the correction coefficient is 0.75. When the difference is greater than 1, the correction coefficient is 0.45. The smaller the difference, the larger the correction coefficient, while the correction coefficient value is 1 when the difference is zero.

Add up by rows, as follows:

$$w_i = \sum_{i=1}^n \bar{b}_{ij}. \tag{10}$$

Normalization by rows, as follows:

$$w_i = \frac{\bar{w}_i \varphi_i}{\sum_{i=1}^n \bar{w}_i \varphi_i}. \tag{11}$$

Obtain the vector  $W = (w_1, w_2, \dots, w_n)^T$ , the characteristic vectors of the judgment matrix, the weight values of the factors.

The consistency test of the judgment matrix is performed using the formula

$$CR = \frac{CI}{RI}, \tag{12}$$

where CR is the consistency ratio of the judgment matrix, CI is the consistency index, and RI is the random consistency index. The value of RI is taken according to Table 2, and CI is calculated using the formula

$$CI = \frac{\lambda_{max} - n}{n - 1}, \tag{13}$$

$$\lambda_{max} = \frac{1}{n} \sum_{j=1}^n \frac{(BW)_i}{w_i}, \tag{14}$$

As the calculated CR value is less than 0.1, the judgment is valid; conversely, the indirect judgment matrix C needs to be modified until the CR value is less than 0.1.

**Table 2.** RI values.

Matrix Order	1	2	3	4	5
RI	0	0	0.52	0.89	1.12

### 2.2.2. Entropy Method

The entropy method is an objective method for assigning values, and its application avoids the influence of human factors on the results. After subjective weights were calculated, the objective weights of the factors were calculated using the entropy method in the following steps:

With  $n \times m$  actual data of  $n$  evaluation factors, the evaluation matrix is

$$R = (y_{ij})_{n \times m}. \tag{15}$$

Standardized using the formula

$$y'_{ij} = \frac{y_{ij} - \min_i(y_{ij})}{\max_i(y_{ij}) - \min_i(y_{ij})}, \tag{16}$$

where the value of  $y_{ij}$  is between 0 and 1.

The entropy of index  $i$  is

$$H_i = -k \sum_{j=1}^m f_{ij} \ln f_{ij}, \tag{17}$$

$$f_{ij} = \frac{y'_{ij}}{\sum_{j=1}^m y'_{ij}}, \tag{18}$$

$$k = \frac{1}{\ln n}, \tag{19}$$

The entropy weight value corresponding to the index  $i$  is

$$\beta_i = \frac{1 - H_i}{n - \sum_{i=1}^n H_i}, \tag{20}$$

### 2.2.3. Grey Relational Analysis

Grey relational analysis is an analytical method that quantitatively describes the trend of a system by comparing the geometrical similarity of the reference data columns with the comparison data columns to determine their degree of correlation. It has the capability to reflect the degree of correlation between different sequences, which allows quantitative analysis of the impact of each risk assessment indicator on the assessment results.

The steps of grey relational analysis are as follows:

#### 1. Determination of the analytical sequence

The risk assessment grade is defined as a reference sequence reflecting the characteristics of the system, and the risk assessment index is defined as a comparative sequence affecting the system, resulting in the following matrix:

$$[X] = \begin{bmatrix} x_{10} & \cdots & x_{1n} \\ \vdots & \ddots & \vdots \\ x_{m0} & \cdots & x_{mn} \end{bmatrix}, \tag{21}$$

where the first column of the matrix is the parent sequence and columns 2 through  $n$  are the subsequences;

#### 2. Dimensionless processing of data

Due to the different dimensions of each risk assessment index, it is difficult to reach a correct conclusion due to errors when analyzing and comparing. In order to reduce the analytical error caused by the difference in dimensions, the original data are made dimensionless using the initial value method. The initial value method is formulated as follows:

$$X' = \frac{x_{ij}}{\frac{1}{n} \sum_{i=1}^n x_{ij}}, \tag{22}$$

#### 3. Calculation of correlation coefficients

$$\xi_{ij} = \frac{\min \left\{ |x'_{ij} - x'_{i0}| \right\} + \rho \max \left\{ |x'_{ij} - x'_{i0}| \right\}}{|x'_{ij} - x'_{i0}| + \rho \max \left\{ |x'_{ij} - x'_{i0}| \right\}}, \tag{23}$$

where  $\xi_{ij}$  represents the correlation coefficient between the parameter  $i$  of the subsequence  $j$  and the parameter  $j$  of the parent sequence,  $\rho$  is the distinguishing coefficient whose value characterizes the variability between correlation coefficients with a range of [0, 1]. In this paper,  $\rho$  is calculated with a value of 0.5.

#### 4. Correlation calculation

The mean value resulting from homogenization of the correlation coefficient sequence is the correlation degree, as follows:

$$\gamma_{0i} = \frac{1}{n} \sum_{i=1}^n \xi_{ij}. \tag{24}$$

The closer  $\gamma_{01}$  is to 1, the higher the correlation between the two.

#### 2.2.4. Locally Linear Embedding

LLE is a nonlinear dimensionality reduction method that maps sample data from a high-dimensional space to a low-dimensional space, while keeping the structural information of the original data unchanged [44]. The basic idea of LLE is that, for a certain sample point  $X_i$  in the space,  $k$  sample points  $X_i^{(k)}$  can be identified in its neighborhood, which can be sufficiently close to  $X_i$  after combining these  $k$  sample points using a coefficient vector  $w_i$ . The coefficient vector  $w_i$  consists of a set  $w_{ij}, j \in N(i), N(i)$  indicates the set of points in the neighborhood of  $X_i$ , and this set  $w_{ij}$  needs to satisfy formula loss Equation (25)

$$w_i^* = \arg w_i \min \frac{1}{2} \|X_i - w_i X_i^{(k)}\|^2, \tag{25}$$

where  $w_{ij}$  is also recognized as the weight coefficient; and after dimensionality reduction, the projection of a sample point with respect to these  $k$  sample points can still be linearly represented using this vector of coefficients.

The LLE calculation process is as follows:

First, select point  $X_i$  with its  $k$  neighbors  $X_i^{(k)}$ . Assuming that there are  $D$  points in the space, calculate the Euclidean distances between point  $X_i$  and the other  $(D-1)$  points in the space, and based on the calculated Euclidean distances choose the  $k$  points that are closer to point  $X_i$ .

Calculate the weight coefficients  $w_{ij}$  between the sample points and  $X_i^{(k)}$ . Assuming that  $X_i$  is a 1-row,  $m$ -column vector and  $X_i^{(k)}$  is a  $k$ -row,  $m$ -column matrix of  $k$  neighboring points, normalizing the restriction on  $w_{ij}$  as follows:

$$\sum_j w_{ij} = 1, \tag{26}$$

Substituting the above equation into Equation (25) to simplify it and solving it with the Lagrange multiplier method yields

$$w_i^* = \frac{I_{k \times 1}^T S_i^{-1}}{I_{k \times 1}^T S_i^{-1} I_{k \times 1}}, \tag{27}$$

$$S_i = w_i \left( I_{k \times 1} X_i - X_i^{(k)} \right) \left( I_{k \times 1} X_i - X_i^{(k)} \right)^T, \tag{28}$$

where  $I_{k \times 1}$  is all 1 vectors.

Constructing Low-Dimensional Data Collections. Assuming that the low-dimensional projections corresponding to points  $X_i$  and  $X_i^{(k)}$  are  $Y_i$  and  $Y_i^{(k)}$ , and satisfy the same linear relationship, i.e., satisfy the loss equation minimization

$$Y^* = \arg \min_Y \sum_i \|Y_i - w_i^* Y_i^{(k)}\|_2, \tag{29}$$

where  $Y^*$  is a matrix of  $N$  rows and  $d$  columns. The mean of the  $N$  values in each column is set to 0, and the variance is set to 1. Matrixing Equation (29) yields

$$\sum_{i=1}^N \|Y_i - W_i^* Y\|_2 = \text{tr} \left[ Y(E - W)(E - W)^T Y^T \right], \tag{30}$$

where  $W = [W_1^* \ W_2^* \ \dots \ W_N^*]^T$ , constructing the Lagrange equation to solve as follows

$$(E_N - W)(E_N - W)^T Y^T = \lambda Y^T, \tag{31}$$

It can be shown that  $Y$  is a matrix consisting of the characteristic vectors of  $(E_N - W)(E_N - W)^T$ .

### 2.2.5. Radial Basis Function Network

RBF is a typical feed-forward neural network, including an input layer, hidden layer, and output layer, and its basic function is to activate the hidden layer neurons through the radial basis function, mapping the original data in the low-dimensional space to the high-dimensional space, so that the original data are transformed from linearly indistinguishable to linearly divisible, to achieve the purpose of training and learning. Compared to general neural networks, such as BP neural networks, it has a faster computational speed and learning capability.

RBF mostly works with a Gaussian function as the activation function of the hidden layer, whose expression is

$$R(x_k - x_i) = \exp\left(-\frac{1}{2\sigma_i^2}\|x_k - x_i\|^2\right), \quad (32)$$

where  $x_k$  is the  $k$  input sample,  $x_i$  is the  $i$  centroid, and  $\sigma_i$  is the width parameter of the function.

The RBF utilizes an interpolation function as the approximation function, which is expressed as

$$F(x) = \sum_{k=1}^n w_k R(x_k - x_i). \quad (33)$$

The output of the network obtained by the RBF neural network is as follows:

$$y_i = \sum_{i=1}^n w_{ij} R(x_k - x_i) \quad (34)$$

## 3. Case Study

### 3.1. The Project

The excavation of Qingdao Metro Anshan Road Station is located at the northwest corner of the intersection of Anshan Road and Shandong Road, and the form is in the shape of an “L”, as shown in Figure 2, and is the deepest station in Qingdao, with a maximum excavation depth of about 42 m. Figure 3 shows the geologic profile of YDK7 + 495.533 – YDK7 + 670.333 of the Anshan Road station excavation. The topography of the area is relatively flat, and the geology is a typical composite stratum of Qingdao area with upper soft and lower hard strata. While the upper soil layer mainly consists of fill, powdery clay, and coarse sand, the lower bedrock is dominated by granite with different degrees of weathering, partially intruded by lamprophyre, granite, and cataclasite. Under the influence of the Guanshan Fracture and Qingdao Mountain Fracture, a number of tectonic fracture zones have been formed at the site, as shown in Figure 4, which are characterized by the development of rock joints and fissures, rock fragmentation, and instability. The depth of the groundwater is about 2.2–4.8 m, which is mainly stored in the fill soil layer and coarse sand layer with strong permeability, recharged through atmospheric precipitation and groundwater seepage. The station was excavated using top-down construction, and the support system is a composite support form, consisting of steel pipe piles, cables, and rock bolts.

During excavation, the existence of fractured rock and joints in the tectonic fracture zone is prone to destabilizing the slope of the excavation. Meanwhile, the surrounding environment of the excavation is complex, being adjacent to schools, residential areas, and viaducts, as shown in Figure 2. The north and northwest sides of the station are adjacent to the school's depot and a residential building, respectively, with a space of 12.5 m and 24 m. And on the west of the excavation are Anshan 4th Road 2A and Qingdao 16th Middle School, with the shortest distances of 20 m and 36.2 m to the excavation. Shandong Road Viaduct and Hang-An Expressway Viaduct are located to the east and south of the excavation, and the distance between the excavation and them is 24.9 m and 22.2 m,

respectively. Additionally, there are 17 underground pipelines within the construction impact area. In particular, as an interchange station, Anshan Road Station has a complex structure with 21 supporting units containing a large number of corners, as shown in Figure 5, which leads to collision of anchors and difficulties in construction control. For the above reasons, during the construction, while ensuring the safety of the excavation itself, it is also necessary to ensure the safety of the surrounding buildings, which greatly increases the difficulty of the project. In fact, the excavation has resulted in cracks in the surrounding ground and buildings, as shown in Figure 6. Therefore, an effective stability assessment is urgently needed to ensure the safety of the excavation.

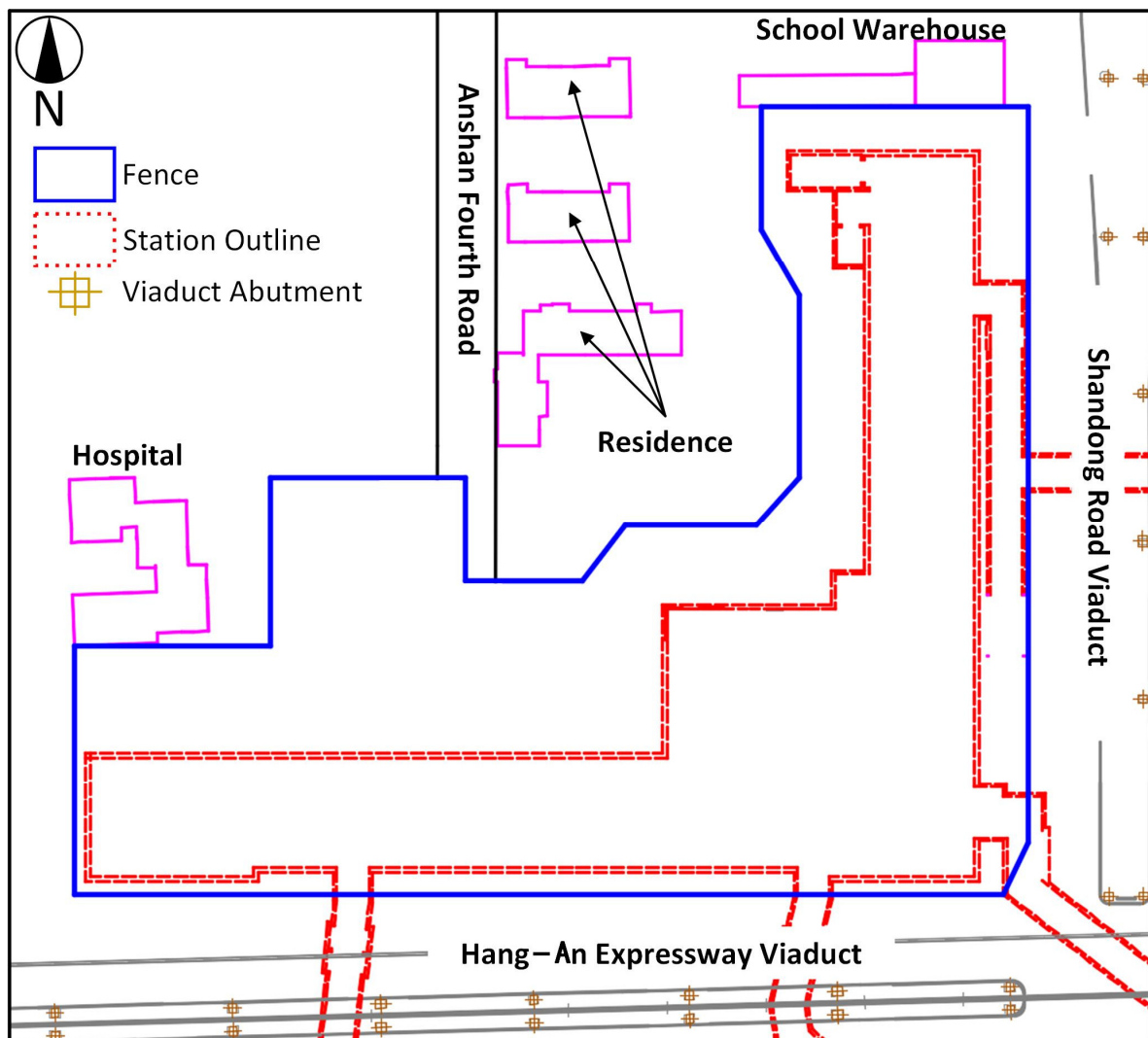


Figure 2. Plan of Anshan Road station.

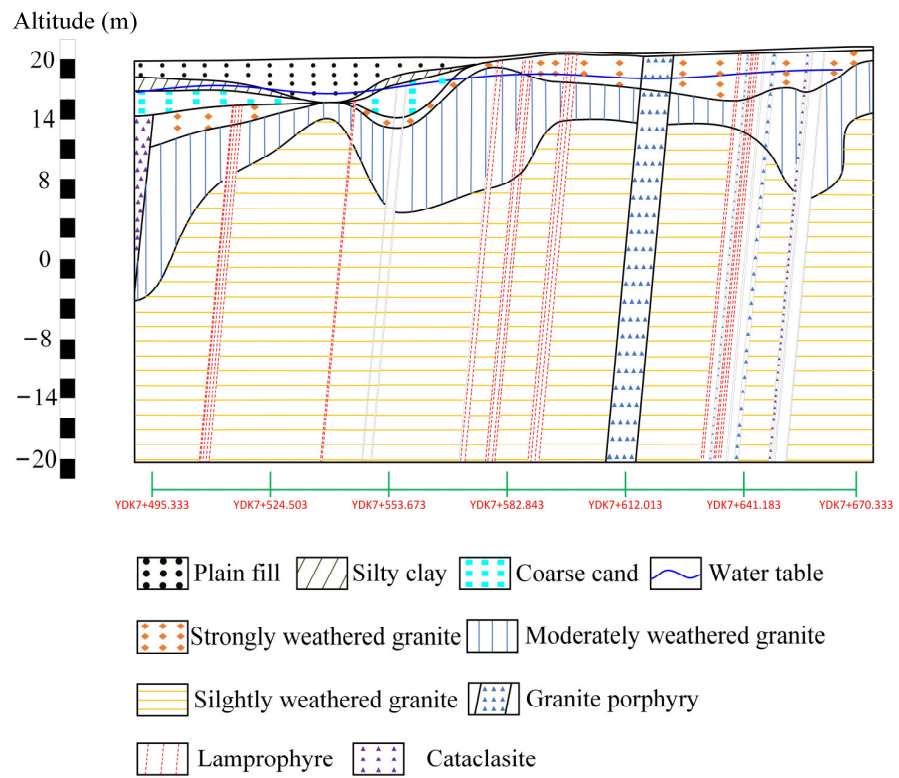


Figure 3. Geological profile.

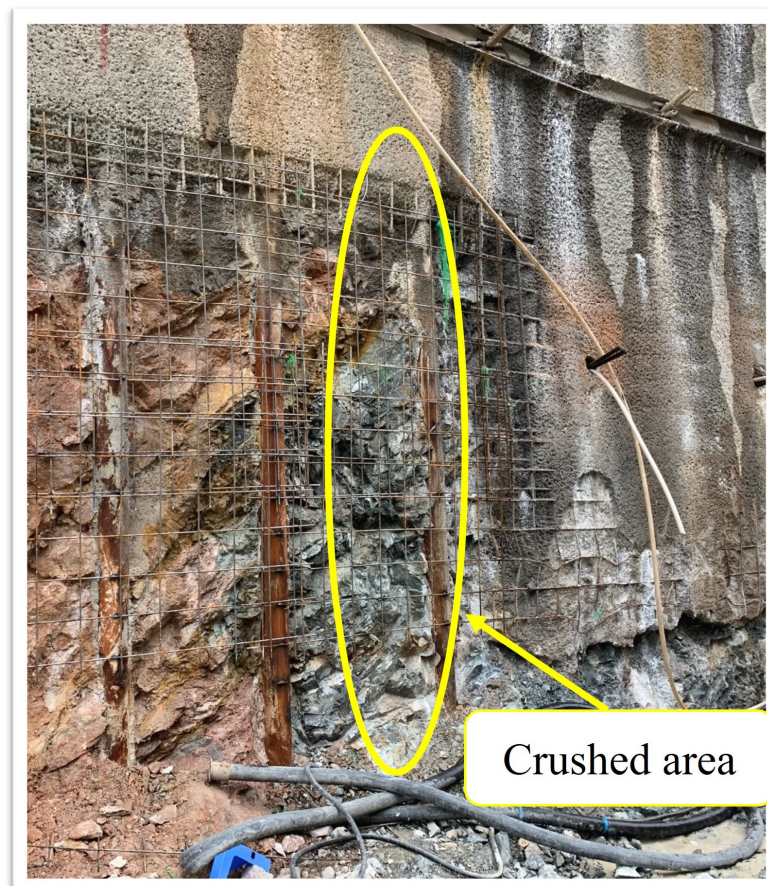


Figure 4. Crushed area.

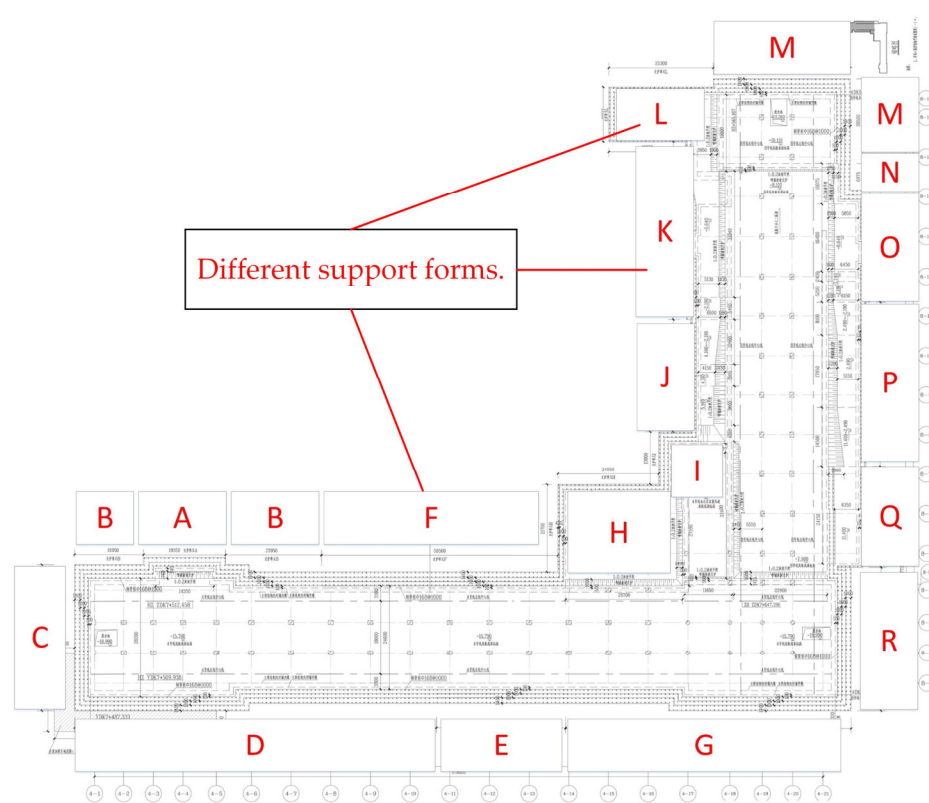


Figure 5. Distribution of support units.

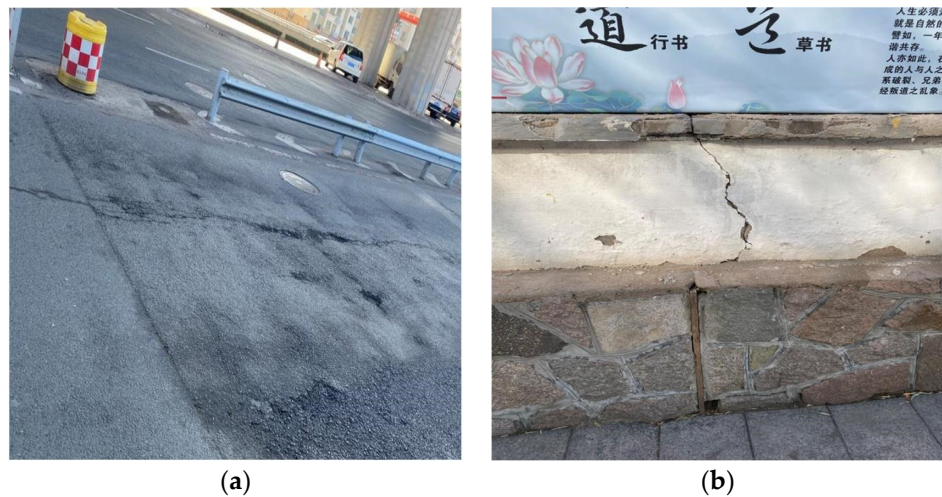


Figure 6. Cracks in neighboring buildings caused by the excavation: (a) crack in the ground; (b) cracks in a wall.

### 3.2. Excavation Risk Assessment

#### 3.2.1. Evaluation Index System for Excavation Instability Risk

The aim of this paper was to construct a model that can dynamically assess the risk of excavation. For this reason, several factors that reflect the dynamic changes in excavation needed to be explored and utilized. The existing research shows that on-site monitoring can well reflect the working condition of rock and supports, which reflects the dynamic changes in excavation engineering [45,46]. Therefore, on-site monitoring programs were considered as risk assessment indexes. In the excavation introduced in Section 3.1, a variety of monitoring programs were undertaken. With the help of invited experts, some of

these were selected as evaluation indexes, including deformation, stress, and microseismic signals. These can dynamically reflect not only the changes in the excavation but also the internal failure of the rock mass. Based on this, while considering the geological characteristics, a risk factor library was established, as shown in Table 3. This consists of 12 potential risk factors under three guideline layer factors, for the environment in the excavation, the environment around the excavation, and the excavation support structure. The useful factor ratio (UR) was used to analyze the importance of each risk factor for the risk evaluation system of deep and large excavations with a soil–rock combination. Thirty experts were invited to judge the importance of the factors through anonymous voting, and the quantified UR is shown in Table 3.

**Table 3.** Potential risk factors and UR values.

Guideline Layer	Potential Risk Factors	UR	Judgements
The environment in the excavation	Soil stress C <sub>11</sub>	0.9	Fit
	Microseismic grade C <sub>12</sub>	0.81	Fit
	Weak rock thickness C <sub>13</sub>	0.67	Fit
	Microseismic frequency C <sub>14</sub>	0.67	Fit
	Special strata C <sub>15</sub>	0.3	Unfit
The environment around the excavation	Thickness of overburden C <sub>21</sub>	0.9	Fit
	Deformation of neighboring buildings C <sub>22</sub>	0.81	Fit
	Surface settlement C <sub>23</sub>	0.7	Fit
	Water table C <sub>24</sub>	0.67	Fit
The excavation support structure	Vertical deformation C <sub>31</sub>	0.81	Fit
	Transverse deformation C <sub>32</sub>	0.81	Fit
	Anchor cable axial force C <sub>33</sub>	0.83	Fit

After the calculation, the factor C<sub>15</sub> named special stratum was not considered in further calculations, owing to the fact that the UR value was less than 0.4. Then, the combined weights of the selected potential risk factors were calculated using the AHP-entropy method. Three experts were selected to perform two-by-two comparisons of the importance between the factors of each layer and quantify their importance according to the Table 1, to establish a judgment matrix. The weight, eigenvector, CR values, entropy value, entropy weight, and comprehensive weight of each expert scoring result were calculated, as shown in Table 4.

**Table 4.** Weights of risk indexes.

	Expert 1	Expert 2	Expert 3	Average Weight	CR	Entropy Value	Entropy Weight	Comprehensive Weight
C <sub>11</sub>	0.23	0.17	0.23	0.21	<0.1	0.934	0.036	0.199
C <sub>12</sub>	0.14	0.17	0.14	0.15		0.811	0.104	0.141
C <sub>13</sub>	0.49	0.33	0.49	0.44		0.934	0.036	0.435
C <sub>14</sub>	0.14	0.33	0.14	0.2		0.680	0.177	0.193
C <sub>21</sub>	0.09	0.11	0.11	0.1		0.931	0.038	0.086
C <sub>22</sub>	0.66	0.54	0.45	0.55	<0.1	0.979	0.012	0.548
C <sub>23</sub>	0.17	0.18	0.34	0.23		0.727	0.151	0.208
C <sub>24</sub>	0.08	0.18	0.10	0.12		0.583	0.231	0.166
C <sub>31</sub>	0.27	0.31	0.43	0.34	<0.1	0.922	0.043	0.317
C <sub>32</sub>	0.27	0.58	0.43	0.43		0.879	0.067	0.386
C <sub>33</sub>	0.46	0.11	0.14	0.23		0.811	0.104	0.206

Twenty experts were invited to score the potential risk factors based on the evaluation set V, to create an original data matrix. For the deep and large excavation with soil–rock combination stability evaluation set V = (V1, V2, V3, V4) = (I, II, III, IV), the original data matrix R was obtained. The original data matrix were standardized and normalized, and

then the entropy value and entropy weight value of each index factor were obtained. The subjective weights and objective weights were integrated and weighted to determine the integrated weights of each indicator factor. It can be seen from Table 4 that the comprehensive weights of the 11 potential risk factors were all greater than 0.1; therefore, they were selected as the risk evaluation index, as shown in Table 5.

**Table 5.** Risk evaluation index system.

Evaluation Index		I	II	III	IV
Soil stress $C_{11}$	MPa	$\leq 6$	6	15	24
Microseismic grade $C_{12}$	grade	$\leq 3$	4	5	$\geq 6$
Weak rock thickness $C_{13}$	m	$< 6$	6–12	12–18	$> 18$
Microseismic frequency $C_{14}$	grade	weak	medium	comparatively strong	strong
Thickness of overburden $C_{21}$	mm	$< 2$	2–5	5–8	$> 8$
Deformation of neighboring buildings $C_{22}$	mm	$< 10$	10–14	14–18	$> 18$
Surface settlement $C_{23}$	mm	$< 12$	12–18	18–24	$> 24$
Water table $C_{24}$	mm	$< 500$	500–1000	1000–1500	$> 1500$
Vertical deformation $C_{31}$	mm	$< 18$	18–24	24–30	$> 30$
Transverse deformation $C_{32}$	mm	$< 12$	12–17	17–25	$> 25$
Anchor cable axial force $C_{33}$	MPa	$< 216$	216–243	243–270	$> 270$

In Table 5, the risk levels are graded based on the different evaluation criteria. First, based on the control criteria defined in the code [47,48], the maximum (minimum) value of the class IV risk was determined. Then, the maximum (minimum) value was subdivided into different ranges with the assistance of the experts, to correspond to different risk levels. In addition, appropriate management measures were set up based on the established evaluation criteria, as shown in Table 6. Finally, the risk evaluation system for deep and large excavation with soil-rock combination was established, as shown in Figure 7.

**Table 6.** Risk classification of excavation.

Risk Level	Management Measures
I	Continue construction and perform daily monitoring.
II	Construction continues with more frequent monitoring and prohibit construction overruns.
III	Construction is suspended with monitoring, while meetings are held to investigate the cause and prepare contingency measures.
IV	Stop construction and all personnel leave, while analyzing the cause, make an early warning and develop measures according to the emergency plan.

Grey relational analysis was used to calculate the correlation between each risk index and the risk level, so as to verify the rationality of its selection. Taking the risk level as the parent series and the values of quantitative indexes as the sub-sequence, after the indexes were made dimensionless, the gray correlation coefficients between the sub-sequence and the parameters of the parent series were calculated as shown in Table 7. The results show that the correlation coefficient of each sub-sequence risk factor index was more than 0.6, which had a strong correlation with the risk level of the parent sequence, so the risk evaluation system for deep and large excavation with soil-rock combination had been selected reasonably.

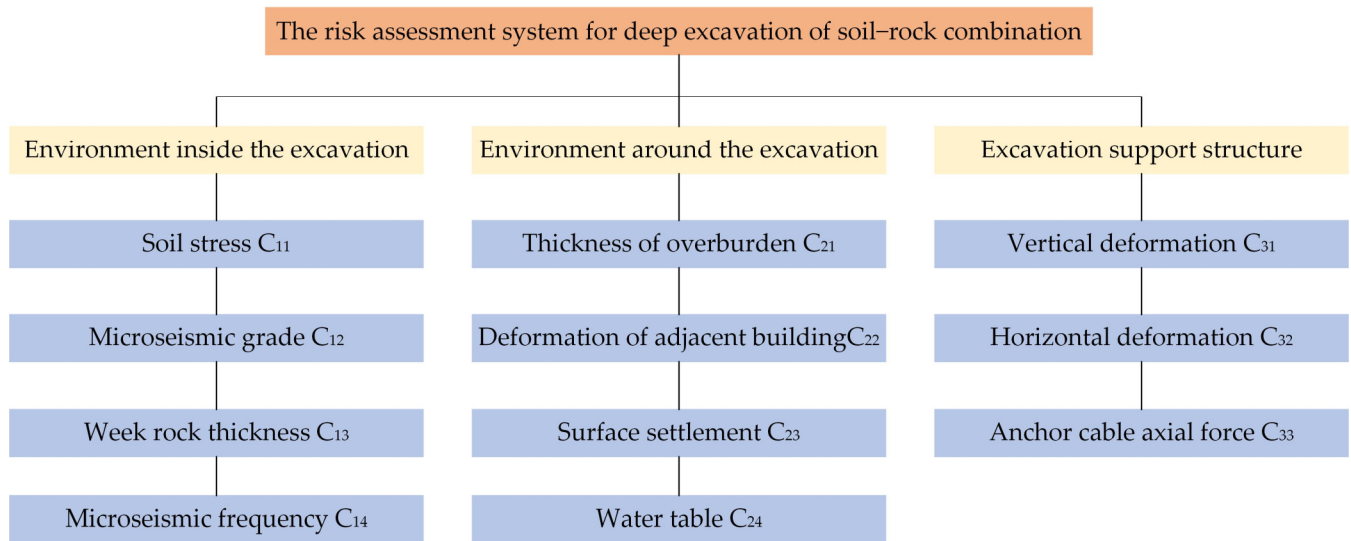


Figure 7. The risk evaluation system.

Table 7. Gray correlation coefficient.

Parent Sequence	Correlation Coefficient											
	C <sub>11</sub>	C <sub>12</sub>	C <sub>13</sub>	C <sub>14</sub>	C <sub>21</sub>	C <sub>22</sub>	C <sub>23</sub>	C <sub>24</sub>	C <sub>31</sub>	C <sub>32</sub>	C <sub>33</sub>	
I	0.9271	0.9119	0.9882	0.4541	0.8392	0.9359	0.7927	0.7798	0.9024	0.9690	0.7823	
II	0.7665	0.7747	0.9766	0.6940	1.0000	0.8589	0.6889	0.9084	0.8253	0.8067	0.6673	
III	0.9271	0.9330	0.8267	0.9455	0.7229	0.8203	0.7235	0.9520	0.8269	0.8281	0.7272	
IV	0.9271	0.9551	0.8267	0.4541	1.0000	0.8203	0.9642	0.9520	0.9558	0.9690	0.8954	

### 3.2.2. Risk Assessment Process Based on Improved Neural Networks

In this paper, 12 sets of data were collected as training data for the RBF network, which are shown in Table 8. The source of these data was the materials provided by the construction company, including geologic investigation reports, construction plans, and monitoring diaries, etc. Therefore, these data were reliable and credible. Moreover, it should be noted that when choosing the LLE algorithm as a method for data dimensionality reduction, the data dimensions should be no less than the number of indexes.

Table 8. Training data.

Risk Level	Quantified Indexes											
	C <sub>11</sub>	C <sub>12</sub>	C <sub>13</sub>	C <sub>14</sub>	C <sub>21</sub>	C <sub>22</sub>	C <sub>23</sub>	C <sub>24</sub>	C <sub>31</sub>	C <sub>32</sub>	C <sub>33</sub>	
1	II	7.87	1.0	7.90	0.54	12.32	-2.95	-7.65	-5869	-11.04	12.29	275.83
2	III	10.23	1.86	10.78	0.57	17.30	-1.88	-5.0	-5711	-8.74	15.09	294.06
3	I	6.16	0.45	4.32	0.37	8.09	-3.58	-9.36	-6015	-12.36	9.60	264.22
4	IV	11.67	1.56	10.96	0.68	19.68	-1.77	-6.45	-5569	-9.85	9.8	257.35
5	II	5.47	2	8.45	0.60	17.68	-2.25	-7.65	-5671	-10.31	9.84	260.43
6	IV	11.16	1.69	10.22	0.81	22.70	-4.63	-9.23	-6423	-11.71	14.49	273.3
7	II	3.77	1.21	5.77	0.35	8.96	-1.5	-8.45	-5848	-11.29	12.26	269.91
8	II	3.64	0.68	5.44	0.20	4.89	-3.71	-10.06	-6377	-12.21	14.91	274.59
9	IV	5.63	1.05	9.54	0.55	10.48	-4.22	-10.95	-7196	-12.26	15.64	301.45
10	III	8.37	0.96	4.58	0.49	8.54	-4.84	-10.91	-6981	-13.09	15.32	287.46
11	I	3.55	0.18	3.27	0.31	6.78	-1.39	-4.47	-5067	-8.38	8.49	254.61
12	IV	10.51	1.93	10.87	0.74	19.64	-1.61	-6.26	-5169	-9.44	14.03	295.47

The original data needed to be processed by applying the LLE algorithm before inputting it into the RBF network. In Table 8, each dataset contains 11 factors with high

dimensionality and non-linearity. Therefore, the dimensionality of the low-dimensional dataset was set to 11 when the data dimensionality was reduced using the LLE algorithm. Twelve sets of training data were input into the neural network, with 1, 2, 3, and 4 used to indicate low risk, medium risk, high risk, and extra high risk, respectively, and the calculation results are shown in Table 8. In Table 9, compared with the actual risk level, the risk level calculated using the model corresponds to it, which indicates that the improved neural network had a high accuracy.

Table 9. Comparison of forecast results.

	Risk Level											
Predicted results	2	3	1	4	2	4	2	2	4	3	1	4
Actual result	II	III	I	IV	II	IV	II	II	IV	III	I	IV

After the neural network was trained, it was used for excavation risk assessment. The monitoring data of Anshan Road pit unit K on 10 January 2019 and 30 May 2019, which had a large cumulative variation, were selected to be used as samples for predicting the safety status of the excavation, as shown in Table 10. Meanwhile, to demonstrate the accuracy of the assessment results, the traditional RBF neural network model, BP neural network model, and fuzzy comprehensive assessment model were used for prediction based on the same data, and the results of the model comparison are shown in Table 11. It can be seen from Table 11 that the prediction results of the improved neural network model corresponded to the actual engineering grades, whose risk for deep excavation on 10 January 2019 and 30 May 2019 were grade II and grade III, respectively.

Table 10. Monitoring data of Unit K.

Date	Horizontal Displacement of Pile Top	Pile Settlement	Deep Horizontal Displacement	Anchor Cable Stress	Surface Settlement	Building Settlement	Water Table
10 January 2019	9.80 mm	−9.85 mm	17.84 mm	257.35 kN	−6.45 mm	−1.77 mm	−5569 mm
30 May 2019	15.38 mm	−13.45 mm	18.72 mm	304.71 kN	−11.56 mm	−5.43 mm	−7151.00 mm

Table 11. Assessment results of different models.

Date	Fuzzy Synthetic Evaluation Model	LLE-RBF	RBF	BP
10 January 2019	II	II	II	III
30 May 2019	III	III	II	III
mean square error		0.045	0.251	0.779

In Table 11, the prediction results of the BP neural network are all class II, which is more conservative. This is because 12 sets of data as training samples are not enough for a BP neural network. This means that the improved RBF network could obtain good results with less information. On the other hand, the traditional RBF networks seemed to have better prediction results, with their risk levels all being 2. However, by comparing the mean square error of the models, the improved model had a smaller value. Incidentally, the BP model had the largest mean square error, with a value of 0.779. This indicates that the improved model had a greater ability to analyze nonlinear factors, and it had a stronger ability to resist interference when abnormal data were present. Overall, the improved model had a higher accuracy and stronger immunity to interference.

Dynamic assessment of excavation risks and taking appropriate measures are significant for ensuring excavation safety. At this point, according to the management measures under the different risk levels listed in Table 6, the monitoring frequency of the pit itself as well as the surrounding environment should be increased during the excavation process.

An important fact to recognize is that the model presented in this paper has many shortcomings requiring improvement. The first point is that the library of potential risk factors needs to be supplemented with more risk factors. In actual engineering, the factors affecting excavation safety are numerous and complex. For example, human factors have a very significant impact on excavation safety but were not included in the factor library developed in this paper. Second, although we tried as far as possible to avoid the role of subjective factors in the factor selection process, their influence was still not completely negligible. The issue of how to solve this problem is an important direction that needs to be focused on in the future. Third, more training samples need to be collected. When the risk factor index increases, the LLE algorithm will no longer be applicable if the number of datasets is insufficient.

#### 4. Conclusions

This study combined a variety of theories to construct a dynamic evaluation model for calculating the instability risk of deep excavation with a soil–rock combination. A stability assessment of the Anshan Road foundation excavation was carried out using the improved RBF neural network, which verified the effectiveness of the proposed model. The main conclusions are as follows:

1. The combined weights method is effective in screening potential risk factors. In this paper, a factor selection model was first constructed. The UR was used for the preliminary identification of potential risk factors. Then, the AHP-entropy method was applied to calculate the combined weights of the factors, with which the risk factors were selected. This factor selection model was valid, as verified through gray correlation analysis;
2. An excavation risk evaluation index system was established for dynamic assessment. The dynamic evaluation of excavation safety was realized based on the improved RBF network, using real-time monitoring data as an evaluation index. A risk assessment of unit K was conducted and the risk grades at 10 January 2019 and 30 May 2019 were class II and class III, respectively. Additionally, comparison of the prediction results with different models verified the validity of the proposed model. The model in this paper had better accuracy and was less dependent on the original data.
3. The model needs further improvement. The model could dynamically analyze the influence of each factor on the risk level of a deep excavation with soil–rock combination in construction. This has significant value in preventing excavation disasters and reducing unnecessary losses. However, a number of drawbacks remain, limiting further applications. This model needs to be gradually improved through continuous application.

**Author Contributions:** Conceptualization, L.Z., Z.W. and S.L.; methodology, L.Z. and S.L.; software, W.Z.; validation, K.L.; formal analysis, W.Z. and K.L.; investigation, L.Z. and Z.W.; data curation, W.Z. and K.L.; writing—original draft preparation, L.Z., W.Z. and Z.W.; writing—review and editing, S.L.; supervision, L.Z.; funding acquisition, Z.W. All authors have read and agreed to the published version of the manuscript.

**Funding:** This research was funded by the Demonstration Project of Benefiting People with Science and Technology of Qingdao, China (Grant No. 23-2-8-cspz-13-nsh), the Shandong Provincial Natural Science Foundation, China (Grant No. ZR2022QD102), the National Natural Science Foundation of China, China (Grant No. 42272334), the Open Project Program of Engineering Research Center of Concrete Technology under Marine Environment, Ministry of Education, China (Grant No. TMduracon2022029).

**Institutional Review Board Statement:** Not applicable.

**Informed Consent Statement:** Not applicable.

**Data Availability Statement:** The datasets generated and/or analyzed during the current study are available from the corresponding author upon reasonable request. The data are not publicly available due to privacy.

**Conflicts of Interest:** The authors declare no conflict of interest.

## References

1. Lin, S.S.; Shen, S.L.; Zhou, A.; Xu, Y.S. Risk assessment and management of excavation system based on fuzzy set theory and machine learning methods. *Autom. Constr.* **2021**, *122*, 103490. [[CrossRef](#)]
2. Liu, J.C.; Tan, Y. Review of through-wall leaking incidents during excavation of the subway stations of Nantong metro line 1 in thick water-rich sandy strata. *Tunn. Undergr. Space Technol.* **2023**, *135*, 105056. [[CrossRef](#)]
3. Huang, L.W.; Xu, Y.L.; Zhou, K.; Wang, G.W. Analysis on the collapse causes of foundation pit under complex environmental in soft soil areas. *Chin. J. Undergr. Space Eng.* **2023**.
4. Wang, K.; Gao, Y.; Jin, Z.; Zhou, X.; Chen, L.; Zhang, C. Research on stability of steep bank slope and reserved thin-walled rock cofferdam during excavation of intake foundation pit. *Eng. Fail. Anal.* **2022**, *141*, 106659. [[CrossRef](#)]
5. Oztoprak, S.; Cinicioglu, S.F.; Oztorun, N.K.; Alhan, C. Impact of neighbouring deep excavation on high-rise sun plaza building and its surrounding. *Eng. Fail. Anal.* **2020**, *111*, 104495. [[CrossRef](#)]
6. Sousa, R.L.; Einstein, H.H. Lessons from accidents during tunnel construction. *Tunn. Undergr. Space Technol.* **2021**, *113*, 103916. [[CrossRef](#)]
7. Zhao, Y.; Chen, X.; Hu, B.; Huang, L.; Lu, G.; Yao, H. Automatic monitoring and control of excavation disturbance of an ultra-deep foundation pit extremely adjacent to metro tunnels. *Tunn. Undergr. Space Technol.* **2023**, *142*, 105445. [[CrossRef](#)]
8. Li, Y.; Zhou, G.; Li, T.; Tang, C.; Gong, B.; Wang, K. Influence of tunnel excavation on the deformation of a frame building. *Buildings* **2023**, *13*, 810. [[CrossRef](#)]
9. Liang, Z.; Gong, B.; Wu, X.; Zhang, Y.; Tang, C. Influence of principal stresses on failure behavior of underground openings. *Chin. J. Rock Mech. Eng.* **2015**, *34*, 3176–3187.
10. Liang, Z.; Gong, B.; Li, W. Instability analysis of a deep tunnel under triaxial loads using a three-dimensional numerical method with strength reduction method. *Tunn. Undergr. Space Technol.* **2019**, *86*, 51–62. [[CrossRef](#)]
11. Chen, B.; Gong, B.; Wang, S.; Tang, C. Research on zonal disintegration characteristics and failure mechanisms of deep tunnel in jointed rock mass with strength reduction method. *Mathematics* **2022**, *10*, 922. [[CrossRef](#)]
12. Zhang, Y.; Zhang, W.; Xia, H.; Gong, B.; Liu, F.; Zhang, J.; Liu, K. Case Study and Risk Assessment of Water Inrush Disaster in Qingdao Metro Line 4. *Appl. Sci.* **2023**, *13*, 3384. [[CrossRef](#)]
13. Finno, R.J.; Bryson, S.; Calvello, M. Performance of a stiff support system in soft clay. *J. Geotech. Geoenviron. Eng.* **2002**, *128*, 660–671. [[CrossRef](#)]
14. Son, M.; Cording, E.J. Estimation of building damage due to excavation-induced ground movements. *J. Geotech. Geoenviron. Eng.* **2005**, *131*, 162–177. [[CrossRef](#)]
15. Shen, S.L.; Lin, S.S.; Zhou, A. A cloud model-based approach for risk analysis of excavation system. *Reliab. Eng. Syst. Saf.* **2023**, *231*, 108984. [[CrossRef](#)]
16. Zhang, X.; An, J. A new pre-assessment model for failure-probability-based-planning by neural network. *J. Loss Prev. Process Ind.* **2023**, *81*, 104908. [[CrossRef](#)]
17. Zhao, J.; Ritter, S.; DeJong, M.J. Early-stage assessment of structural damage caused by braced excavations: Uncertainty quantification and a probabilistic analysis approach. *Tunn. Undergr. Space Technol.* **2022**, *125*, 104499. [[CrossRef](#)]
18. Choi, H.H.; Cho, H.N.; Seo, J.W. Risk assessment methodology for underground construction projects. *J. Constr. Eng. Manag.* **2004**, *130*, 258–272. [[CrossRef](#)]
19. Zhou, H.B.; Zhang, H. Risk assessment methodology for a deep foundation pit construction project in Shanghai, China. *J. Constr. Eng. Manag.* **2011**, *137*, 1185–1194. [[CrossRef](#)]
20. Zhou, Y.; Li, S.; Zhou, C.; Luo, H. Intelligent approach based on random forest for safety risk prediction of deep foundation pit in subway stations. *J. Comput. Civ. Eng.* **2019**, *33*, 05018004. [[CrossRef](#)]
21. Gong, B.; Tang, C.A.; Wang, S.Y.; Bai, H.M.; Li, Y.C. Simulation of the nonlinear mechanical behaviors of jointed rock masses based on the improved discontinuous deformation and displacement method. *Int. J. Rock Mech. Min. Sci.* **2019**, *122*, 104076. [[CrossRef](#)]
22. Feng, X.H.; Gong, B.; Cheng, X.F.; Zhang, H.H.; Tang, C.A. Anisotropy and microcrack-induced failure precursor of shales under dynamic splitting. *Geomat. Nat. Hazards Risk* **2022**, *13*, 2864–2889. [[CrossRef](#)]
23. Wang, Y.Y.; Gong, B.; Tang, C.A. Numerical investigation on anisotropy and shape effect of mechanical properties of columnar jointed basalts containing transverse joints. *Rock Mech. Rock Eng.* **2022**, *55*, 7191–7222. [[CrossRef](#)]
24. Wang, Y.; Gong, B.; Zhang, Y.; Yang, X.; Tang, C. Progressive fracture behavior and acoustic emission release of CJBs affected by joint distance ratio. *Mathematics* **2022**, *10*, 4149. [[CrossRef](#)]
25. Liang, Z.; Gong, B.; Tang, C.; Zhang, Y.; Ma, T. Displacement back analysis for a high slope of the Dagangshan Hydroelectric Power Station based on BP neural network and particle swarm optimization. *Sci. World J.* **2014**, *2014*, 741323. [[CrossRef](#)]
26. Chen, X.S.; Hong, C.Y.; Su, D. Intelligent geotechnical engineering. *Chin. J. Geotech. Eng.* **2022**, *44*, 2151–2159.

27. Hegde, J.; Rokseth, B. Applications of machine learning methods for engineering risk assessment-A review. *Saf. Sci.* **2020**, *122*, 104492. [[CrossRef](#)]
28. Gong, B. Study of PLSR-BP model for stability assessment of loess slope based on particle swarm optimization. *Sci. Rep.* **2021**, *11*, 17888. [[CrossRef](#)]
29. Zhang, C.; Li, J.Z.; He, Y. Application of optimized grey discrete Verhulst–BP neural network model in settlement prediction of foundation pit. *Environ. Earth Sci.* **2019**, *78*, 441. [[CrossRef](#)]
30. Shen, Y.S.; Wang, P.; Li, M.P.; Mei, Q.W. Application of subway foundation pit engineering risk assessment: A case study of Qingdao rock area, China. *KSCE J. Civ. Eng.* **2019**, *23*, 4621–4630. [[CrossRef](#)]
31. Lin, S.S.; Zhang, N.; Zhou, A.; Shen, S.L. Risk evaluation of excavation based on fuzzy decision-making model. *Autom. Constr.* **2022**, *136*, 104143. [[CrossRef](#)]
32. Sou-Sen, L.; Hsien-Chuang, L. Neural-network-based regression model of ground surface settlement induced by deep excavation. *Autom. Constr.* **2004**, *13*, 279–289. [[CrossRef](#)]
33. Li, X.; Pan, Y.; Zhang, L.; Chen, J. Dynamic and explainable deep learning-based risk prediction on adjacent building induced by deep excavation. *Tunn. Undergr. Space Technol.* **2023**, *140*, 105243. [[CrossRef](#)]
34. Lü, Q.; Chan, C.L.; Low, B.K. Probabilistic evaluation of ground-support interaction for deep rock excavation using artificial neural network and uniform design. *Tunn. Undergr. Space Technol.* **2012**, *32*, 1–18. [[CrossRef](#)]
35. Kounlavong, K.; Keawsawasvong, S.; Wipulanusat, W.; Jamsawang, P. Physics-based and data-driven modeling for basal stability evaluation of braced excavations in natural clays. *Heliyon* **2023**, *9*, 10.
36. Ning, X.; An, Y.; Ju, L.; Wang, W. Real-time online prediction of surface settlement considering spatiotemporal characteristics during foundation excavation. *Autom. Constr.* **2023**, *150*, 104831. [[CrossRef](#)]
37. Tang, Y.; Xiao, S.; Zhan, Y. Predicting settlement along railway due to excavation using empirical method and neural networks. *Soils Found.* **2019**, *59*, 1037–1051. [[CrossRef](#)]
38. Tao, Y.; Sun, H.; Cai, Y. Predictions of deep excavation responses considering model uncertainty: Integrating BiLSTM neural networks with Bayesian updating. *Int. J. Geomech.* **2022**, *22*, 04021250. [[CrossRef](#)]
39. Liu, Y.; Yang, Z.; Li, X. Adaptive ensemble learning of radial basis functions for efficient geotechnical reliability analysis. *Comput. Geotech.* **2022**, *146*, 104753. [[CrossRef](#)]
40. Huang, Z.K.; Zhang, D.M.; Xie, X.C. A practical ANN model for predicting the excavation-induced tunnel horizontal displacement in soft soils. *Undergr. Space* **2022**, *7*, 278–293. [[CrossRef](#)]
41. Chen, R.P.; Zhang, P.; Kang, X.; Zhong, Z.Q.; Liu, Y.; Wu, H.N. Prediction of maximum surface settlement caused by earth pressure balance (EPB) shield tunneling with ANN methods. *Soils Found.* **2019**, *59*, 284–295. [[CrossRef](#)]
42. Liu, B.; Wang, R.; Zhao, G.; Guo, X.; Wang, Y.; Li, J.; Wang, S. Prediction of rock mass parameters in the TBM tunnel based on BP neural network integrated simulated annealing algorithm. *Tunn. Undergr. Space Technol.* **2020**, *95*, 103103. [[CrossRef](#)]
43. Zhang, R.; Tian, D.; Wang, H.; Kang, X.; Wang, G.; Xu, L. Risk Assessment of Compound Dynamic Disaster Based on AHP-EWM. *Appl. Sci.* **2023**, *13*, 10137. [[CrossRef](#)]
44. Chen, J.; Liu, Y. Locally linear embedding: A survey. *Artif. Intell. Rev.* **2011**, *36*, 29–48. [[CrossRef](#)]
45. Kavvadas, M.J. Monitoring ground deformation in tunnelling: Current practice in transportation tunnels. *Eng. Geol.* **2005**, *79*, 93–113. [[CrossRef](#)]
46. Masini, L.; Gaudio, D.; Rampello, S.; Romani, E. Observed performance of a deep excavation in the historical center of Rome. *J. Geotech. Geoenviron. Eng.* **2021**, *147*, 05020015. [[CrossRef](#)]
47. GB 50497-2009; Technical Standard for Monitoring of Building Excavation Engineering. Ministry of Housing and Urban-Rural Development of the People’s Republic of China, Planning Publishing House: Beijing, China, 2009.
48. GB 50911-2013; Code for Monitoring Measurement of Urban Rail Transit Engineering. Ministry of Housing and Urban-Rural Development of the People’s Republic of China, China Architecture & Building Press: Beijing, China, 2014.

**Disclaimer/Publisher’s Note:** The statements, opinions and data contained in all publications are solely those of the individual author(s) and contributor(s) and not of MDPI and/or the editor(s). MDPI and/or the editor(s) disclaim responsibility for any injury to people or property resulting from any ideas, methods, instructions or products referred to in the content.